

Bioinspired durable interpenetrating network anti-icing coatings enabled by binders and hydrophobic-ion specific synergies

Shen Zhang^a, Feng Gao^{a,b,*}, Zhiqin Jiang^a, Qinggang He^{a,b}, Jianguo Lu^c, Yang Hou^{a,b,c}, Xiaoli Zhan^{a,b,c}, Qinghua Zhang^{a,b,c,*}

^a Zhejiang Provincial Key Laboratory of Advanced Chemical Engineering Manufacture Technology, College of Chemical and Biochemical Engineering, Zhejiang University, Hangzhou 310027, China

^b Institute of Zhejiang University-Qzhou, Zhejiang Provincial Innovation Center of Advanced Chemicals Technology, Quzhou 324000, China

^c Donghai Laboratory of Zhejiang University, Zhoushan 316000, China



ARTICLE INFO

Keywords:

Antifreeze proteins
Anti-icing
Interpenetrating coatings
Deicing
Self-cleaning
Synergistic

ABSTRACT

Designing a coating with a comprehensive range of anti-icing properties is a difficult challenge in the current complex and variable icing environment. Bionic anti-icing coatings have received widespread attention in recent years, but their exposure to mechanical damage conditions tends to result in insufficient durability. This work proposes a novel approach inspired by the antifreeze proteins (AFPs) found in fish, wherein a durable interpenetrating coating with excellent anti-icing and deicing performance is designed by combining a fluorinated amphiphilic ionic polymer with a biomimetic binder. The incorporation of hydrophobic fluorinated chain segments and amphiphilic ionic chain segments effectively inhibits ice nucleation ($DT = 2010$ s, $T_{IN} = -22.1$ °C), slows down ice propagation, and reduces ice adhesion ($\tau = 22.2$ kPa) through the synergistic effect of hydrophobicity and ionic specificity. Furthermore, the addition of a bionic binder to create an interpenetrating network enhances the mechanical properties and anti-icing durability of the coating. Moreover, it can further function as anti-fogging, self-cleaning, and antibacterial for glass surfaces, demonstrating significant potential in the new generation of optical and medical devices.

1. Introduction

Icing or frost is one of the most common phenomena in nature, but icing and frost on solid surfaces can lead to many inconveniences to industrial production as well as personal life. For example, icing on the surfaces of power transmission lines, wind turbine blades, roads, aircraft, solar panels, and ships can impede their normal functioning and give rise to safety concerns [1–5]. Active anti-icing methods based on deicing agents [6,7], heating [8], and mechanical deicing tend to be time-consuming and energy-consuming [9], inefficient, and potentially harmful to the environment. In contrast, passive anti-icing methods, which modify surface properties to reduce ice accumulation, offer a more sustainable solution [10].

Human survival and development is an ongoing process of selecting or designing biomimetic materials inspired by nature to resist environmental changes and challenges. For example, early superhydrophobic surfaces (SHSs) inspired by rose petals and lotus leaves, etc. [11–16],

can effectively repel water droplets and inhibit ice nucleation. However, their preparation often requires substrate treatment to form complex artificial surface microstructures, which are not universally applicable. Furthermore, the interlocking effect of liquid-filled cavities at high humidity increases adhesion strength [17], and the surface rough structure is easily destroyed during deicing [18,19]. Smooth liquid-injected porous surfaces (SLIPS) inspired by piggybacking significantly reduce ice adhesion due to the low surface energy of the liquid film and extremely low coefficient of friction [20–24]. However, loss of lubricant can lead to surface performance failure. Electrolyte brushes (PB) [25] and polyelectrolyte brushes (PEM) [26] can modulate the ice nucleation and propagation properties by modifying counter ions, but the poor mechanical properties limit their large-scale practical application.

Considering the significance of the ice-substrate interface for ice adhesion [27], the focus should shift from static surfaces to dynamic changes in the chemical and physical state of the ice-substrate interface [28]. Although a non-freezing water layer at the ice-solid contact

* Corresponding authors at: Zhejiang Provincial Key Laboratory of Advanced Chemical Engineering Manufacture Technology, College of Chemical and Biochemical Engineering, Zhejiang University, Hangzhou, 310027, China.

E-mail addresses: gf933168@163.com (F. Gao), qhzhang@zju.edu.cn (Q. Zhang).

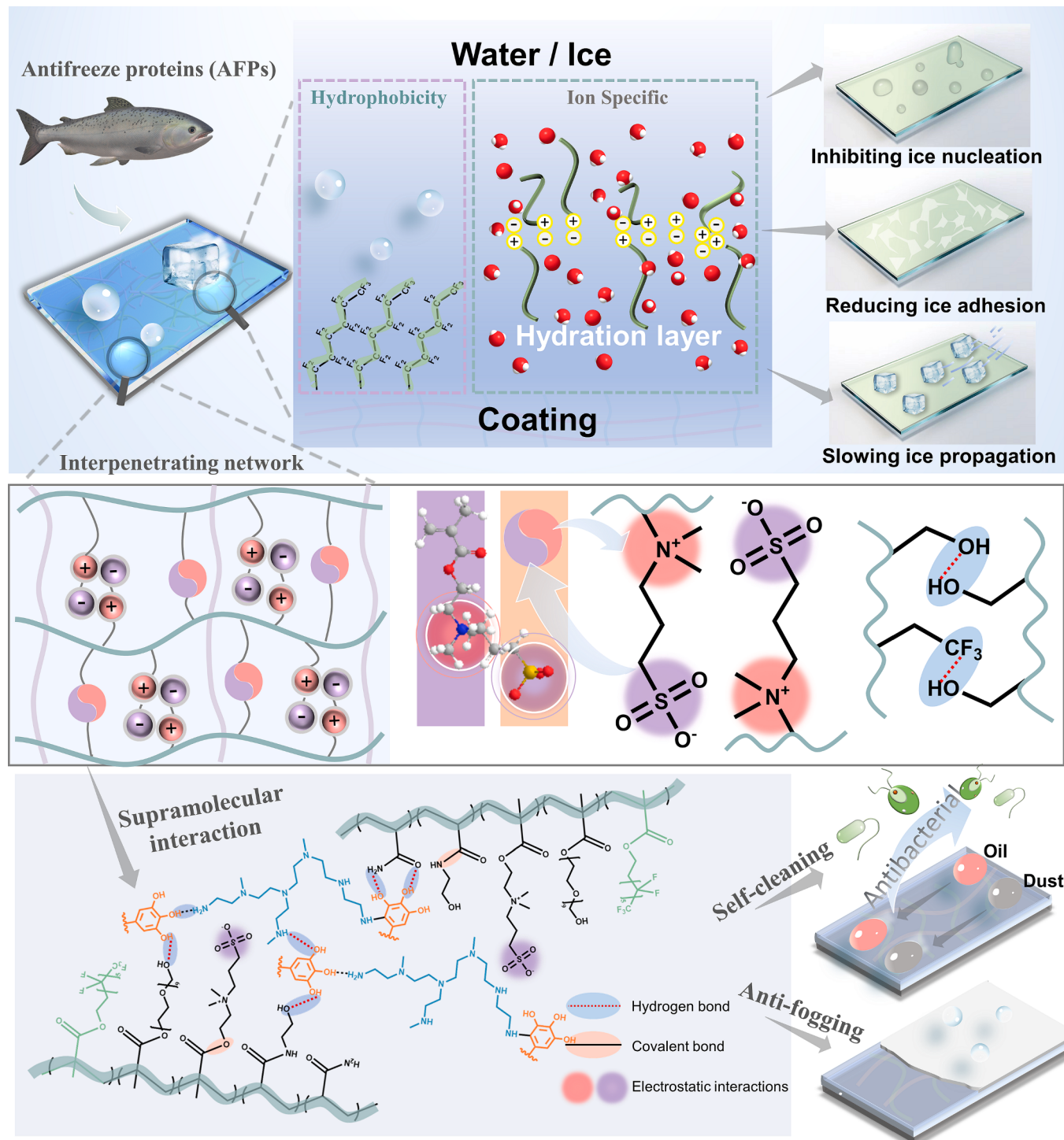


Fig. 1. Design and adaptive interpenetrating network of anti-icing coatings inspired by natural antifreeze proteins.

interface was discovered as early as 2004, its mechanism was not explored and applied to anti-icing until much later [29]. Drawing inspiration from cryobiology and bio-adaptation, antifreeze proteins (AFPs) in polar animals, such as Arctic fish [30], can enhance their antifreeze properties by selectively adsorbing to the surface of ice crystals and by adjusting the properties of interfacial water to inhibit ice nucleation, growth and adhesion. It is now found that the interfacial water can be controlled by adjusting the arrangement of hydrophobic and charged functional groups [31–33]. However, the exposure of such materials to mechanical damage conditions is prone to graft polymer chain failure and insufficient durability. Ideally, an efficient ice-sparing

surface should have multiple anti-icing functions to meet the challenges posed by different environments and address all of the aforementioned problems. Therefore, it is crucial to determine how to incorporate well-balanced hydrophilic and hydrophobic components to regulate the properties of the interfacial water and design a network structure to maintain the mechanical durability of the material to achieve comprehensive anti-icing performance that inhibits ice nucleation [34], slows down ice propagation, and reduces ice adhesion.

Herein, inspired by natural antifreeze proteins (AFPs) in fish, anti-icing coating (ASPF-PT) with an adaptive interpenetrating network was designed and fabricated via emulsion polymerization and

subsequent *in situ* interlinked techniques. Unlike the artificial surface microstructure and previous reports that commonly only focused on a single process, its inherent anti-icing advantage comes from the complex network structure design inside the coating that synergistically targets all ice formation processes. More specifically, as shown in Fig. 1, an amphoteric copolymer with a highly branched fluorinated network (ASPF) has been synthesized. Due to its hydrophobic perfluoroalkyl side chains, ASPF coatings have low surface energy, which can inhibit ice nucleation. In particular, hydrophilic [2-(Methacryloyl-oxy)ethyl] dimethyl-(3-sulfopropyl) ammonium hydroxide (SBMA) chain segments can migrate to coating surfaces in high humidity conditions and icing to form a disordered hydrated layer that inhibits ice nucleation and reduces ice adhesion [35–37]. Additionally, we used a complex of branched polyethyleneimine (PEI) and tannic acid (TA) to prepare a bionic adhesive PEI-TA second network. This network interacts with the substrate and the ASPF copolymer network through its inherent bionic bonding ability and has bactericidal functions. In combination with ASPF and PEI-TA, the synergistic interaction of multiple dynamic bonds in this ASPF-PT network matrix makes the coating mechanically durable and can effectively inhibit ice nucleation ($DT = 2010$ s, $T_{IN} = -22.1$ °C), slow down ice propagation and reduce ice adhesion ($\tau = 22.2$ kPa) through hydrophobic and ion-specific synergistic effects, achieving all-around anti-icing. Furthermore, this coating shows potential applications in self-cleaning, anti-fogging, and antibacterial fields.

2. Experimental section

2.1. Materials

Acrylamide (AM, 99 %), Hexadecyltrimethyl ammonium bromide (CTAB, 99 %), [2-(Methacryloyl-oxy)ethyl]dimethyl-(3-sulfopropyl) ammonium hydroxide (SBMA, 97 %), *N*-Hydroxyethylacrylamide (NHEMAA, 98 %), and Tannic acid (TA, 95 %) were purchased from Shanghai Aladdin Biochemical Technology Co., Ltd. Poly (ethylene glycol) monomethacrylate (PEGMA, M_w 950), emulsifier (MOA-9) were obtained from Rhawn Reagent Co., Ltd. 2-(Perfluorohexyl) Ethyl Methacrylate (C_6F) was acquired from Energy Chemical Reagent Co., Ltd. Polyethylenimine branched (PEI, M_w 10000, 98 %) was bought from Beijing Hwrk Chemical Co., Ltd. 2, 2'-azobis[2-methylpropionamidine] dihydrochloride was received from Shanghai Yuanye Biotechnology Co. Ltd. Deionized water was used for all the experiments.

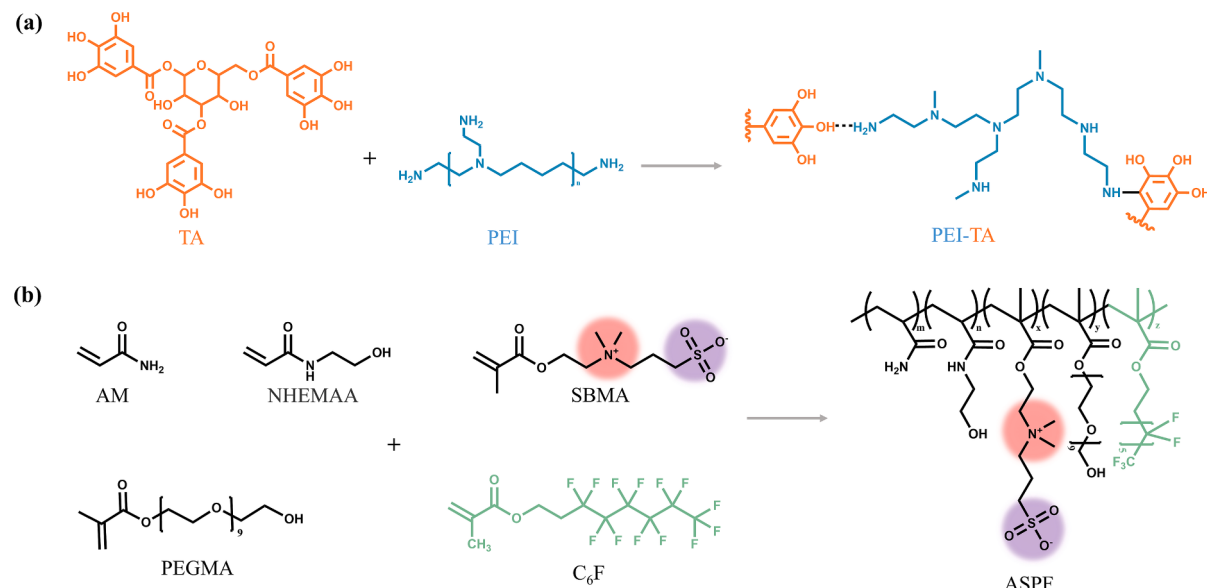


Fig. 2. Synthesis diagram of (a) PEI-TA and (b) ASPF.

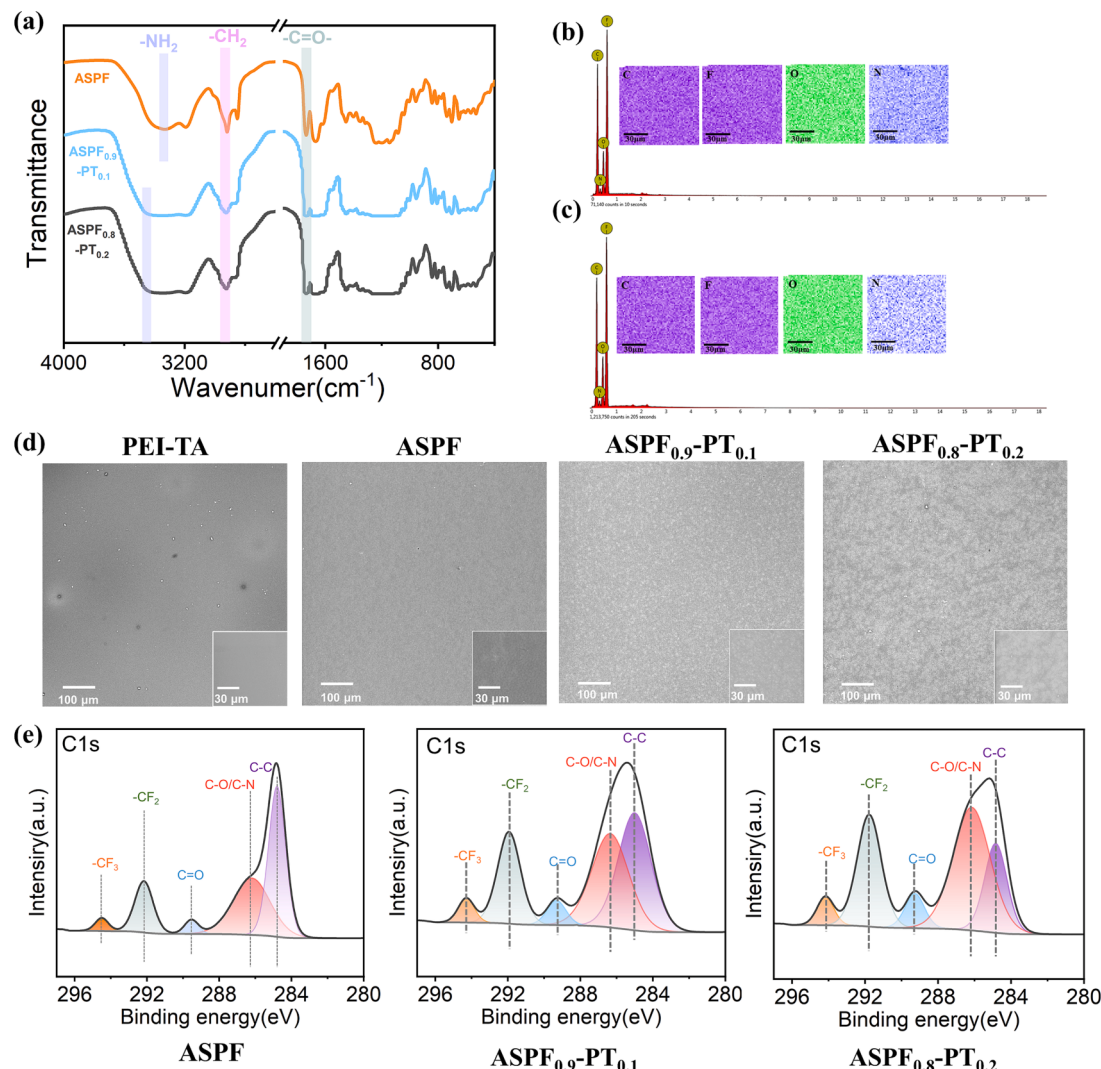


Fig. 3. (a) FTIR spectra of ASPF, ASPF_{0.9}-PT_{0.1}, and ASPF_{0.8}-PT_{0.2}. EDS spectra and corresponding mapping images of (b) ASPF and (c) ASPF_{0.8}-PT_{0.2} coating. (d) SEM images of PEI-TA, ASPF, ASPF_{0.9}-PT_{0.1} and ASPF_{0.8}-PT_{0.2}. (e) XPS C1s spectra of ASPF, ASPF_{0.9}-PT_{0.1}, and ASPF_{0.8}-PT_{0.2} in the dry state.

was characterized by thermogravimetric analyzer (TGA, TA-Q500). The test temperature range was 30–800 °C, the temperature rise rate was 10 °C min⁻¹, and the air atmosphere (flow rate 60 mL min⁻¹). ASPF and ASPF-PT were spin-coated onto a polished silicon wafer to analyze its surface morphology in the wet and dry state under an atomic force microscope (AFM, Multi-Mode, VEECO) in tapping and contacting mode and the root-mean-square (R_{ms}) roughness values of 10 × 10 μm² areas were calculated. The automated tip approach setpoint was 800 mV. Scan rate was 1 Hz. Scan lines were 256. The R_{ms} of a coating was taken the average from five areas chosen randomly.

Details of the characterization are given in the [Supporting Information](#).

3. Results and discussion

3.1. Preparation of anti-icing coatings

We designed the ASPF-PT coatings based on three criteria: (i) droplets are removed in a timely manner, (ii) prevention of ice formation (inhibiting ice nucleation, preventing ice propagation), decrease of ice adhesion, and (iii) exceptional resistance to mechanical damage. The ASPF-PT coating combines the advantages of an interpenetrating network structure. The network of ASPF cross-linked by van der Waals forces acting on highly branched polar/nonpolar functional groups,

hydrogen bonds, and ionic interactions. Additionally, ASPF is based on the study of the structure and antifreeze mechanism of the antifreeze protein (AFP) by grafting hydrophobic chains on hydrophilic charged networks and polymerizing hydrophobic chain segments such as fluorinated acrylate (C₆F) and hydrophilic chain segments such as sulfonic acid betaine amphoteric electrolyte (SBMA). The enrichment of perfluoroalkyl side chains on the surface gives the coating a low surface energy, which effectively inhibits ice nucleation and reduces ice shear strength [38]. Amphiphilic ionic sulfobetaine (SBMA) chain segments as non-ice binding sites can form a hydrated layer with a disordered structure to inhibit ice nucleation and can migrate to the surface of the coating to enhance its hydrophilicity to regulate interfacial water molecules [39], and lower the water freezing point through ionic solvation effect and Hydrogen bonding with water molecules to inhibit ice propagation and diffusion effectively. As a result of a one-step deposition process, polyethylenimine-tannic acid (PEI-TA) complexes can be effectively and stably coated onto substrates while retaining their bio-inspired adhesive properties. Importantly, the biomimetic adhesive PEI-TA facilitates the construction of mechanically durable interpenetrating network coatings. The synthesis process of hydrophobic fluorinated zwitterionic polymer ASPF and hydrophilic multi-hydrogen bonded supramolecular interactions PEI-TA is shown in [Fig. 2](#). The successful synthesis of AF, ASPF, and PEI-TA could be certified by the FTIR in [Figs. S1 and S2 \(Supporting Information\)](#). The incorporation of SBMA in

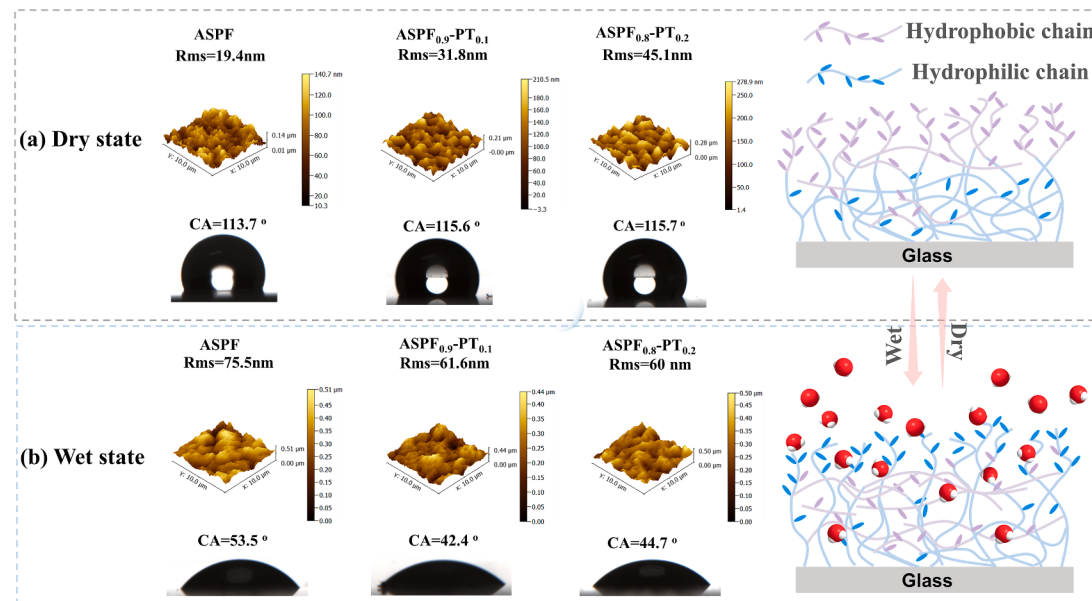


Fig. 4. AFM images and WCA (2 μ L) of ASPF, ASPF_{0.9}-PT_{0.1}, and ASPF_{0.8}-PT_{0.2} coatings under (a) dry and (b) wet state conditions.

the polymeric framework was verified by the observation of characteristic peaks of sulfonic terminals and quaternary ammonium cations of SBMA. Table S1 (Supporting Information) shows the feed mole ratio of the samples prepared (AF, ASPF, PEI-TA, ASPF_{0.9}-PT_{0.1}, and ASPF_{0.8}-PT_{0.2}). Notably, “ASPF-PT” was prepared by ASPF and PEI-TA in different mass ratios, named as “ASPF_x-PT_y” (x and y are the mass fraction of ASPF and PEI-TA: x%, y%). Particularly, the network of PEI-TA coatings displays a smooth surface and high optical transparency (Fig. S3, Supporting Information), which combines the hydrophilicity, antibacterial properties, and biomimetic bonding properties of PEI [40,41] and TA [42].

The chemical structure of ASPF-PT was detected by FTIR in Fig. 3a. Compared to ASPF, the absorption peak of $-\text{NH}_2$ shifted to 3353 cm^{-1} , proving the formation of strong hydrogen bonds between ASPF and PEI-TA. As shown in Fig. 3b, c, elemental analysis showed that the surface of both ASPF and ASPF-PT coatings contained C, F, O, and N elements. The coverage of F elements on the surface of the coatings demonstrated the successful integration of C_6F into the matrix, and the long-chain fluorine migrated and was exposed to the surface of the coating, giving the coating a certain degree of hydrophobic properties. In addition, in order to investigate the changes in surface properties of coatings in high humidity environments such as icing, surface elemental distributions of ASPF and ASPF-PT coatings in the dry and wet states were also investigated (Fig. S4, Supporting Information). Compared with the dry state, the relative content of F elements on the coating surface decreased and the relative content of Oxygen elements increased after 3 h of immersion in water, and a new peak of S appeared in the wet state. These results suggest the migration of hydrophilic chain segments, such as SBMA, to the coating surface in the wet state. Fig. 3d displays the surface topography of all the samples observed by scanning electron microscopy (SEM). The PEI-TA complex formed a smooth and uniform dense coating, and the uniformly distributed C_6F in ASPF and ASPF-PT could cover the hydrogen bonds on the surface of the matrix to reduce ice adhesion [43], which also formed a uniform and smooth surface. The thickness of ASPF_{0.8}-PT_{0.2} coating is shown in Fig. S5 (Supporting Information), is only $136 \pm 3 \mu\text{m}$. Additionally, X-ray photoelectron spectroscopy (XPS) C1s spectra in Fig. S6a (Supporting Information) and Fig. 3e, corresponding to EDS results of ASPF and ASPF-PT samples, demonstrated the presence of C – C, C – N, C – O, C = O, $-\text{CF}_2$ and $-\text{CF}_3$ bonds on ASPF-PT coating surfaces. With the increased PEI-TA content, C – O and C – N content increased, whereas the $-\text{CF}_2$ and

$-\text{CF}_3$ content remained relatively unchanged. Furthermore, ASPF and ASPF-PT coatings were tested in wet state using XPS after being immersed in water for 24 h to examine their surface elements. In the wet state, ASPF and ASPF-PT coatings contained fewer F and more O and N elements, with traces of S elements (Fig. S6b, Fig. S7 and Table S2, Supporting Information). It is proved that the hydrophilic chain segments migrate and distribute to the surface of the coatings in the wet state, which is favorable for forming the hydration layer.

In order to illustrate the phase-separated structure of hydrophilic-hydrophobic chain segments in ASPF-PT coatings and their surface morphology in more depth, we prepared ASPF and ASPF-PT coatings by spin-coating to avoid the effect of thickness on the surface morphology of the coatings. Atomic force microscopy (AFM) was used to detect the surface morphology of the coating under both wet and dry conditions. As shown in Fig. 4a, in the dry state, due to the incompatibility and surface energy difference between the hydrophobic component of C_6F and the hydrophilic component (such as PAAM and PEI-TA, etc.), the C_6F chain segment with low surface energy is easily enriched on the outermost surface of the coating and leads to obvious phase separation domains on the surface with an island-like surface morphology [44,45], with a water contact angle of 113.7°. With the increase of PEI-TA, the phase separation of hydrophilic and hydrophobic chain segments increased, and more obvious phase separation domain and folding morphology appeared on the surface of the coating, with the root mean square roughness (R_{ms}) increased from 19.4 nm (ASPF) to 31.8 nm (ASPF_{0.9}-PT_{0.1}) and 45.1 nm (ASPF_{0.8}-PT_{0.2}), which was more favorable for the homogeneous distribution of the hydrophobic perfluorinated side chains on the surface (which could also be proved by XPS). The ASPF-PT coated surface exhibited hydrophobicity with a water contact angle of 115.7°.

The freezing phenomenon often occurs in wet and low-temperature environments, so the surface morphology of ASPF and ASPF-PT coatings in wet state was also investigated. After being immersed in deionized water for 3 h, as shown in Fig. 4b, the surface micromorphology showed significant differences due to the water-driven surface reorganization of the amphiphilic polymer. Additionally, the migration of hydrophilic chain segments from the interior to the surface of the coating increases the height of this region. Consequently, the R_{ms} of the coating surface increased to 75.5 nm (ASPF), 61.6 nm (ASPF_{0.9}-PT_{0.1}), and 60.0 nm (ASPF_{0.8}-PT_{0.2}), respectively [46].

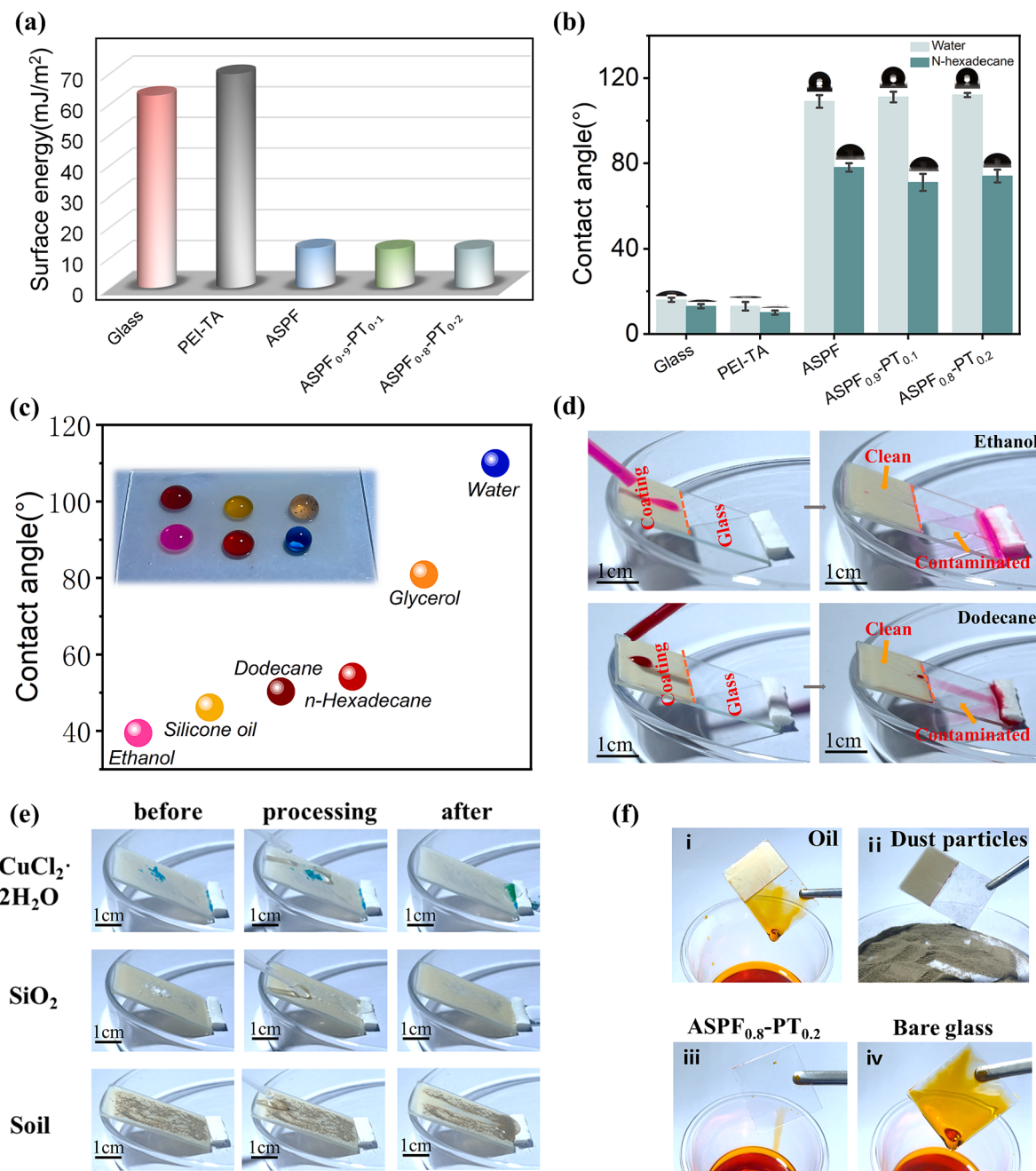


Fig. 5. (a) Surface energy of various coatings. (b) Water (2 μ L) and N-hexadecane contact angle (2 μ L) on glass, steel, ASPF, and ASPF-PT coatings. (c) Photograph and contact angle of various liquid droplets (3 μ L) on the ASPF_{0.8}-PT_{0.2} coating surface. (d) Time-lapse snapshots taken during the sliding of labeled ethanol and dodecane on the ASPF_{0.8}-PT_{0.2} coating and bare glass. Self-cleaning performance of ASPF_{0.8}-PT_{0.2} coating (Slide size: 25 mm \times 37.5 mm) against (e) solid model contaminants. (f) oil (i) and dust particles (ii); Testing the self-cleaning performance of the ASPF_{0.8}-PT_{0.2} coating prepared by spin coating method (iii) and bare glass (iv) in oil.

3.2. Wettability and self-cleaning property

The freezing temperature of hydrophobic surfaces decreases as their surface energy (SE) decreases [47]. As shown in Fig. 5a, both ASPF and ASPF-PT coatings exhibited surface energy within the range of 10—20 mJ m⁻². This can be attributed to the enrichment of perfluoroalkyl side chains on the surface. The ASPF_{0.8}-PT_{0.2} coating surface exhibited a water contact angle of 115.7° (Fig. 5b) and a water sliding angle of 25.2° (Fig. S8, Supporting Information), indicating that water droplets can resist adhesion to the small contact area, resulting in a longer freezing delay [17]. In addition, under high humidity conditions, the coating's smooth surface prevents interlocking between ice crystals and porous

surface structures, thereby reducing ice adhesion [48]. Meanwhile, the wettability of ASPF_{0.8}-PT_{0.2} coatings was evaluated by measuring the contact angle (3 μ L) of various liquids, including water and organic liquids such as ethanol and different oils (Fig. 5c). Generally, the contact angle increases with surface tension enhanced [49]. In comparison to water (0.0728 N m⁻¹), which exhibited a higher CA (115.7°), ethanol had the lowest surface tension (0.0223 N m⁻¹) and exhibited the lowest CA (39.4°). Fig. 5d shows labeled ethanol and dodecane droplets sliding along the tilted ASPF_{0.8}-PT_{0.2} coating without leaving any traces, compared to the blank glass slides that left a lot of liquid sliding traces. According to these results, ASPF_{0.8}-PT_{0.2} coatings can effectively resist oil contamination, which is attributed to its perfluoroalkyl side chains

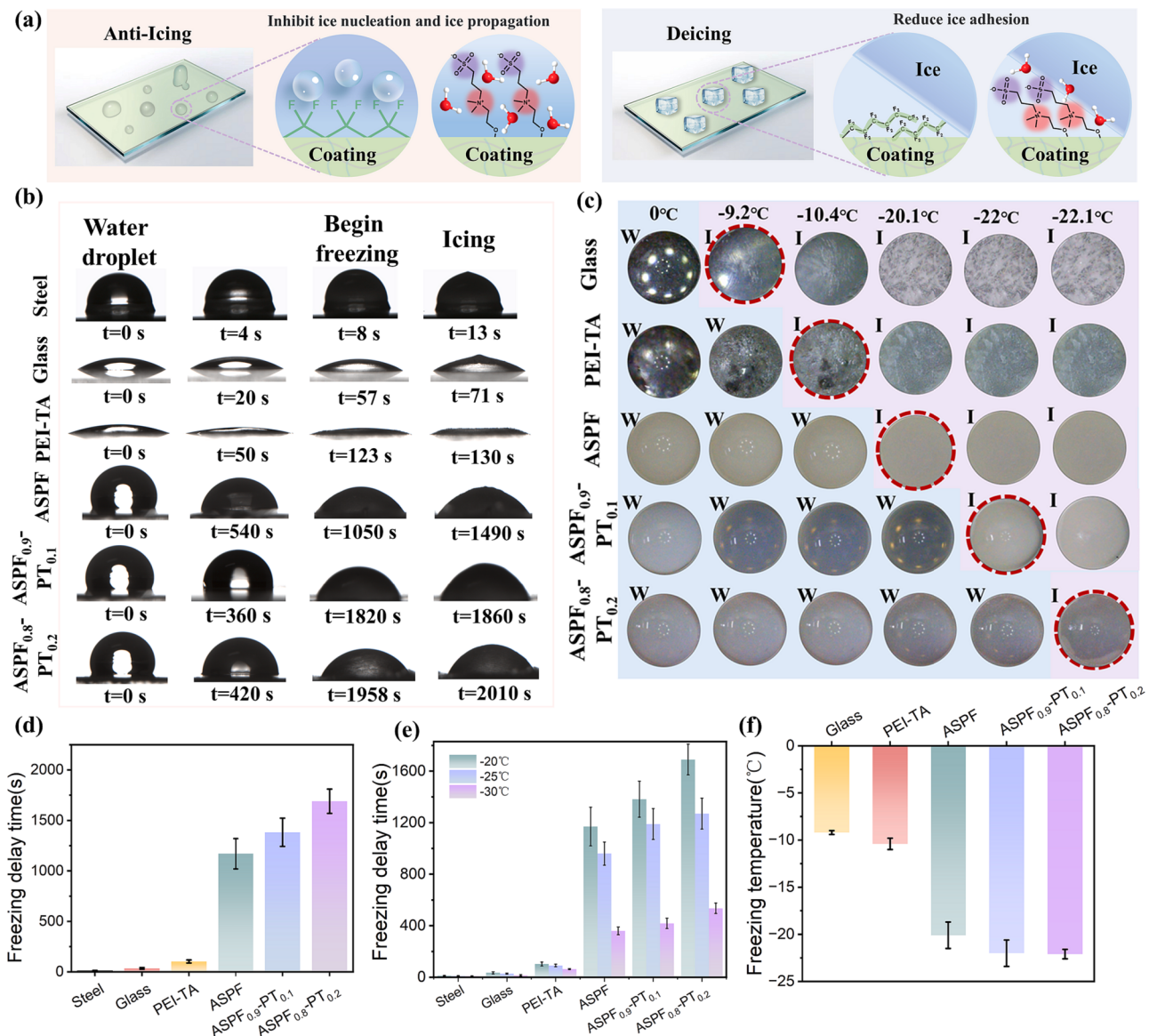


Fig. 6. (a) Schematic diagram of the contact interface between ASPF-PT coating and water. (b) Optical microscope images of water droplets (3 μ L) on glass, steel, PEI-TA, ASPF, and ASPF-PT coatings at -15 $^{\circ}$ C. (c) Optical microscope images of water droplets (5 μ L) on glass, steel, ASPF, and ASPF-PT coatings at a cooling rate of 5 $^{\circ}$ C min $^{-1}$. I, ice; W, water. Scale bar, 1 mm. (d) Freezing delay time (DT) for glass, steel, PEI-TA, ASPF, and ASPF-PT coatings at -15 $^{\circ}$ C. (e) Freezing delay time (DT) for glass, steel, PEI-TA, ASPF, and ASPF-PT coatings at -20 $^{\circ}$ C, -25 $^{\circ}$ C and -30 $^{\circ}$ C. (f) Ice nucleation temperature (T_{IN}).

that are enriched on its surface.

Additionally, we assessed the self-cleaning properties of the coating by using liquid and solid model contaminants, confirming that the ASPF_{0.8}-PT_{0.2} coating resists contamination and adhesion [50]. As shown in Fig. 5e, solid particle contaminants (CuCl₂·2H₂O, SiO₂ powder, and Soil) easily slid off the surface with the flow of water droplets [51,52]. Due to the hydrophobic and oleophobic nature of the per-fluoroalkyl side chain enrichment on the ASPF_{0.8}-PT_{0.2} coating, liquid contaminants like edible oil, honey, and water easily slide off (Fig. S9, Supporting Information). However, the glass became contaminated when liquid contaminants moved along the glass and left residual traces along the travel path. To further visualize the oleophobic performance of the ASPF_{0.8}-PT_{0.2} coating, as shown in Fig. 5f(i), the coating was completely immersed in oil, and the oil can slide off the surface quickly without leaving any trace after removal, compared to the glass, which has been completely contaminated with oil. Fig. 5f(ii) further demonstrates the self-cleaning performance of the ASPF_{0.8}-PT_{0.2} coating after rubbing through solid dust particles. In practice, however, the

preparation of oleophobic coatings often requires some special surface textures, which make the coatings opaque [53–55]. We demonstrate in Fig. 5f (iii, iv) that the ASPF_{0.8}-PT_{0.2} coating prepared by the spin-coating method maintains high transparency while still possessing excellent oleophobic properties, leaving no traces on the surface after being removed from oil immersion, which further improves the practical application range of the coating.

3.3. Anti-Icing/Deicing performance

The icing process is a complex liquid–solid phase change process that always starts with nucleation. With the growth of a stable nucleus, water molecules are continuously transferred from the supercooled liquid into the ice crystals until complete freezing. Therefore, as the first stage and control step of ice formation, the inhibition of ice nucleation facilitates the removal of supercooled water droplets before freezing [56,57]. The interfacial properties of the water/ice-substrate largely determine the anti-icing properties of the surface (Fig. 6a). Here, the anti-icing

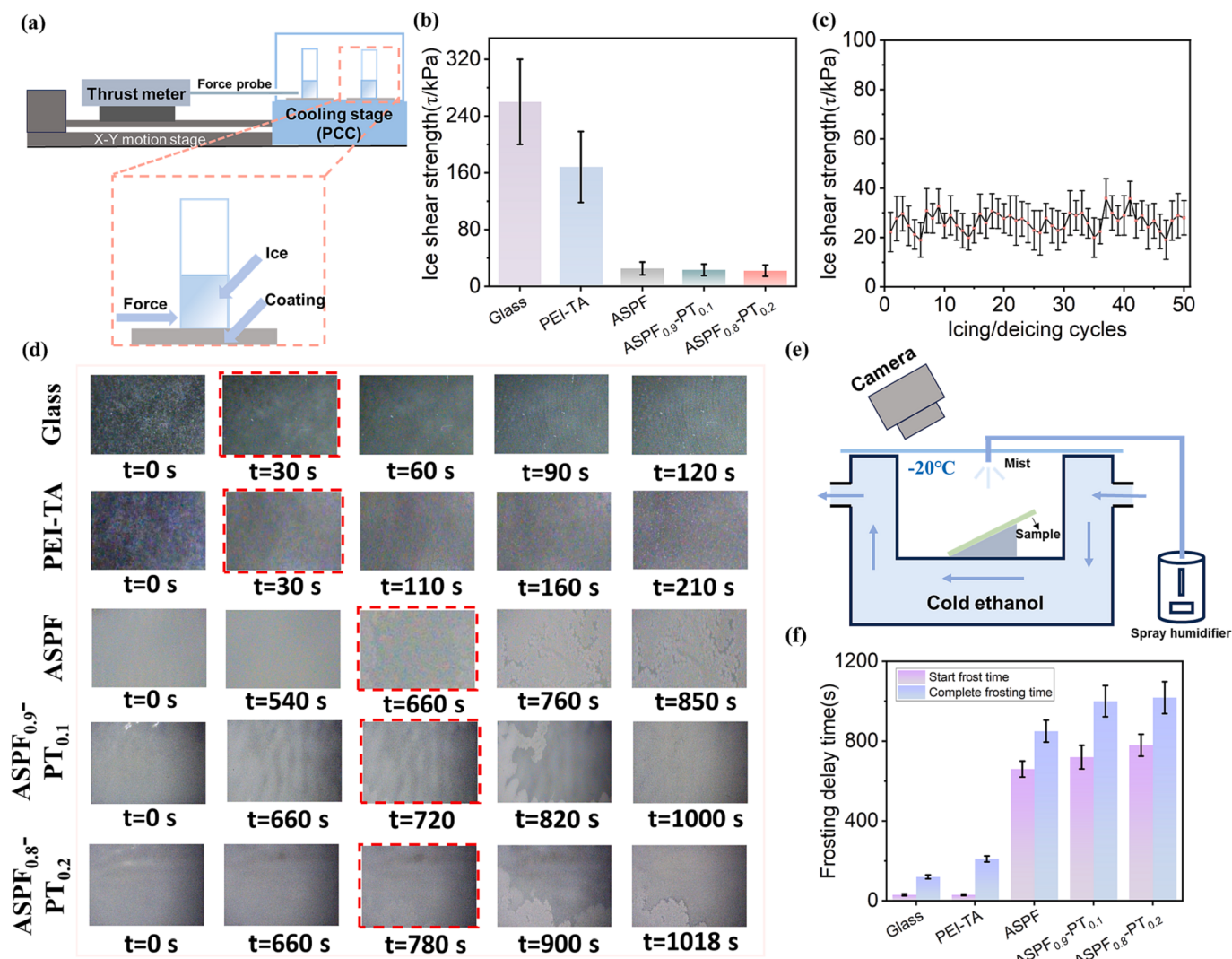


Fig. 7. (a) Schematic diagram of the ice shear strength measurement device. (b) Ice shear strength (τ) on glass, PEI-TA, ASPF and ASPF-PT coatings ($T = -20 \pm 0.5^\circ\text{C}$, Humidity $37 \pm 5\%$). (c) Ice shear strength (τ) on $\text{ASPF}_{0.8}\text{-PT}_{0.2}$ coating during 50 icing/deicing cycles ($T = -20 \pm 0.5^\circ\text{C}$, Humidity $38 \pm 5\%$). (d) Frosting of glass, PEI-TA, ASPF and ASPF-PT coated surfaces over time ($T = -20 \pm 0.5^\circ\text{C}$, Humidity $70 \pm 5\%$). (e) Schematic diagram of the anti-frost measuring device. (f) Frost start time and complete frost time on glass, PEI-TA, ASPF, and ASPF-PT coated surfaces.

performance of the coatings was evaluated by water contact angle (WCA), freezing delay time (DT), and ice nucleation temperature (T_{IN}) tests. As illustrated in Fig. 5b, the surface of the ASPF-PT coating enriched with perfluoroalkyl side chains exhibits hydrophobicity, with WCAs up to 115.7° . DT and T_{IN} revealed the inhibition of ice nucleation on the coating surface. Fig. 6b depicts the freezing process and freezing delay time (DT) of water droplets on the coating at -15°C . It has been observed that the droplets freeze completely once they solidify and develop pointed tips. The DT data are summarized in Fig. 6d. The DT of the superhydrophilic coating PEI-TA (130 s) was 10 and 2 times longer than that of the steel sheet (13 s) and glass (71 s), respectively, compared with the DT of the hydrophobic ASPF coating, which could be extended to 1490 s. Particularly, with the addition of the hydrophilic negatively charged tannic acid (TA) and positively charged polyethylenimine (PEI) network component, the DT of the interpenetrating network ASPF-PT coating was further extended, with the longest DT (2010 s) for the $\text{ASPF}_{0.8}\text{-PT}_{0.2}$ coating being 154 times longer than that of the steel. The DT of the coatings was also evaluated at various temperatures ranging from -20°C to -30°C , as displayed in Fig. 6e, with the same trend as at -15°C . Additionally, we conducted tests to determine the temperature at which ice nucleation first occurs on the coating, referred to as total ice nucleation (T_{IN}), where a lower T_{IN} value suggests a delayed

onset of ice nucleation [34]. Fig. 6c illustrates the ice nucleation process on different surfaces during cooling, with T_{IN} defined as the temperature at which the transparency of the water droplets suddenly changes during the process, and the results are summarized in Fig. 6f. Under uniform cooling conditions, ice nucleation occurred first on the glass ($T_{IN} = -9.2^\circ\text{C}$) and PEI-TA ($T_{IN} = -10.4^\circ\text{C}$) surfaces, while the T_{IN} of the ASPF coating surface could be reduced to -20.1°C . The T_{IN} of the dual-network ASPF-PT coating was further reduced, with the $\text{ASPF}_{0.8}\text{-PT}_{0.2}$ coatings having the lowest T_{IN} (-22.1°C), indicating that the $\text{ASPF}_{0.8}\text{-PT}_{0.2}$ coatings significantly inhibited ice nucleation. It can be assumed that the ice nucleation temperature in this process follows Kelvin's Eq. (1) and Clausius – Clapeyron relation Equation (2), where P and P_0 are the vapor pressure and saturation vapor pressure at a given temperature, respectively. A hydrophobic surface possesses a smaller droplet radius of curvature (r), resulting in an increased vapor pressure P . According to Eq. (2), the change in ice nucleation temperature T is negatively correlated with the change in P since the solidification process is one in which $\Delta V_m > 0$ and $\Delta H_m < 0$ [58]. Compared to the hydrophilic surface, the $\text{ASPF}_{0.8}\text{-PT}_{0.2}$ coated surface exhibits a higher subcooling pressure P , resulting in a lower ice nucleation temperature T .

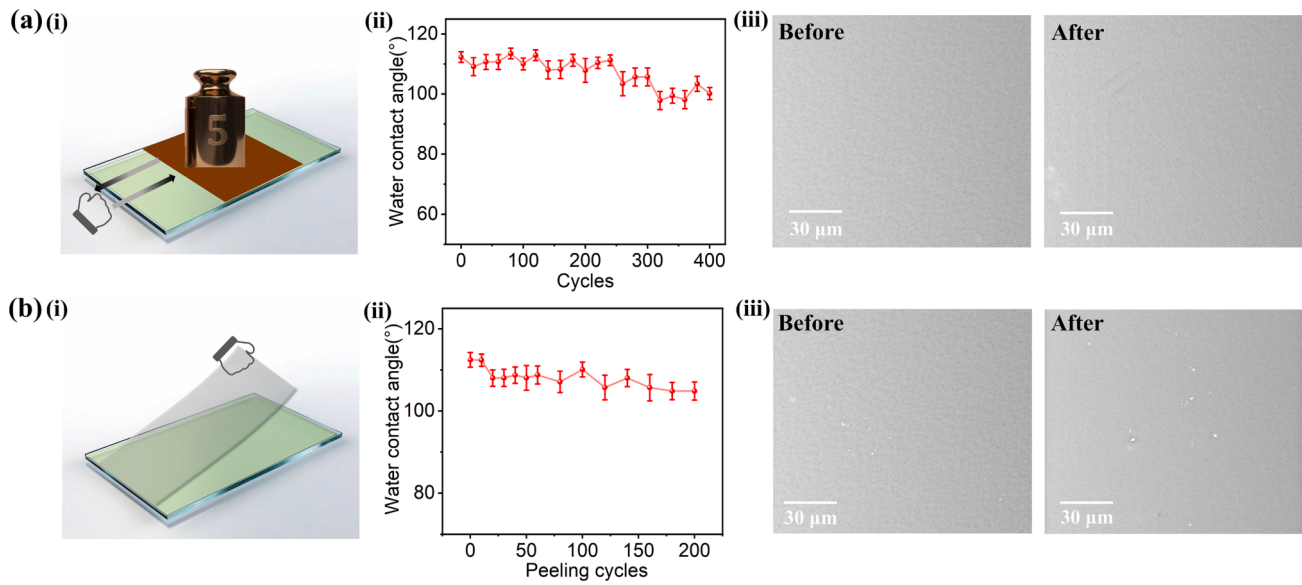


Fig. 8. (a) Diagram of (i) sandpaper abrasion test, (ii) WCAs, and (iii) SEM images of $\text{ASPF}_{0.8}\text{-PT}_{0.2}$ coating before and after 400 cycles test. (b) Diagram of (i) tape peeling test, (ii) WCAs, and (iii) SEM images of $\text{ASPF}_{0.8}\text{-PT}_{0.2}$ coating before and after 200 cycles test.

$$\ln \frac{P}{P_0} = \frac{2\gamma V_m}{R T r} \quad (1)$$

$$\ln \frac{T_2}{T_1} = \frac{\Delta_{\text{sol}} V_m}{\Delta_{\text{sol}} H_m} (P_2 - P_1) \quad (2)$$

While ice on the coating generally undergoes heterogeneous nucleation, according to the classical nucleation theory, the nucleation rate is mainly controlled by the nucleation energy barrier, which in turn is influenced by the subcooling, water contact angle, and surface structure [17]. Eq. (3) shows that a decrease in the contact area of water droplets with the surface and an increase in the contact angle increase the nuclear energy barrier, which leads to a decrease in the ice nucleation rate and a delay in freezing [59].

$$\Delta G = \pi \sigma_{lv} r^2 \frac{(2 - 3 \cos \theta + \cos^3 \theta)}{3} \quad (3)$$

The distribution of fluoroalkyl side chains on the surface of $\text{ASPF}_{0.8}\text{-PT}_{0.2}$ coating results in a higher contact angle and a higher nucleation energy barrier compared to hydrophilic surfaces. The amphoteric SBMA chain segment can form a disordered, hydrated layer that inhibits ice nucleation. In conclusion, $\text{ASPF}_{0.8}\text{-PT}_{0.2}$ can inhibit ice nucleation by modulating the synergistic effect of hydrophobicity and ion specificity.

Ice phobicity refers to a surface's ability to repel or prevent icing and to facilitate the removal of accumulated ice with minimal shear [60], typically requiring an ice shear strength of less than 100 kPa [61]. When the coating surface is covered with ice, the deicing performance of the coating should be further considered. The variation in ice shear strength among different coating surfaces can be attributed to their wetting behavior towards water droplets. We tested the ice shear strength of different coatings (Fig. 7a), and the results are shown in Fig. 7b. At -20°C , the hydrophilic PEI-TA coating and glass could be thoroughly wetted by water and have high adhesion to ice. In contrast, both ASPF and ASPF-PT coatings exhibited an ice shear strength of 20–30 kPa, which significantly decreased due to the hydrophobic perfluoroalkyl side chains reducing the coating's surface energy and minimizing contact area with water droplets. Additionally, the AFP-inspired hydrophilic SBMA chain segment produced a certain amount of non-freezable water at the ice-coating interface, further reducing ice adhesion strength [62].

Compared with ASPF, the addition of hydrophilic network PEI-TA in ASPF-PT coating effectively improves the internal cross-linking of

polymer chains and constructs multiple hydrogen-bonded double networks while intensifying the phase separation of pro-hydrophobic chain segments, which, to some extent is more favorable to the uniform distribution of long-chain fluorine on the surface, as evidenced by XPS and EDS results. To assess the coating's practical application, we investigated the durability of the $\text{ASPF}_{0.8}\text{-PT}_{0.2}$ coating in icing/deicing cycles, as depicted in Fig. 7c. Remarkably, even after 50 icing/deicing cycles at -20°C , the $\text{ASPF}_{0.8}\text{-PT}_{0.2}$ coating's τ remained virtually unaltered. In summary, the ASPF-PT coating can regulate the nature of interfacial water by modulating the synergistic effects of hydrophobicity and ion-specificity, thereby modulating its anti-icing performance.

The frosting process can be viewed as a type of ice propagation process. As the local surface temperature decreases, water molecules on the object's surface gradually condense into small water droplets, interacting with the ice crystals on the surface and promoting their growth [5]. Moreover, water molecules in the air continuously adhere and coalesce on the object's surface through diffusion, leading to the thickening of the frost layer. We further explored the anti-frost properties of the coating (Fig. 7e). Microscopy images of frost on the coating surface at different time points at -20°C are shown in Fig. 7d, and the data are summarized in Fig. 7f. The glass and hydrophilic coating PEI-TA started to frost at 30 s, and the surface was completely covered with frost after 120 s and 210 s, respectively. In contrast, the $\text{ASPF}_{0.8}\text{-PT}_{0.2}$ coating started frosting only at 780 s (26 times more than the glass), and the surface was completely covered with frost after 1018 s. Frosting typically begins at the edges [63], but freezing droplets can also randomly appear inside the surface, influenced by dust particles and other factors that arise during the condensation process.

The anti-frost performance of $\text{ASPF}_{0.8}\text{-PT}_{0.2}$ coating can be explained by the following mechanism: according to Eq. (4), frosting on a smooth hydrophobic coating surface should generally satisfy the condition that the air pressure (P_v) around the condensing droplet is higher than the critical nucleation pressure ($P_{v, \text{sat}}$). Analysis reveals that as the surface contact angle increases, the contact area between the liquid and air increases, thereby improving vapor diffusion around the droplet. Furthermore, it can be inferred from Eq. (1) that the critical nucleation pressure $P_{v, \text{sat}}$ is greater on hydrophobic surfaces than on hydrophilic surfaces (right side of Eq. (4)). This makes it difficult for vapor to condense into frost [64].

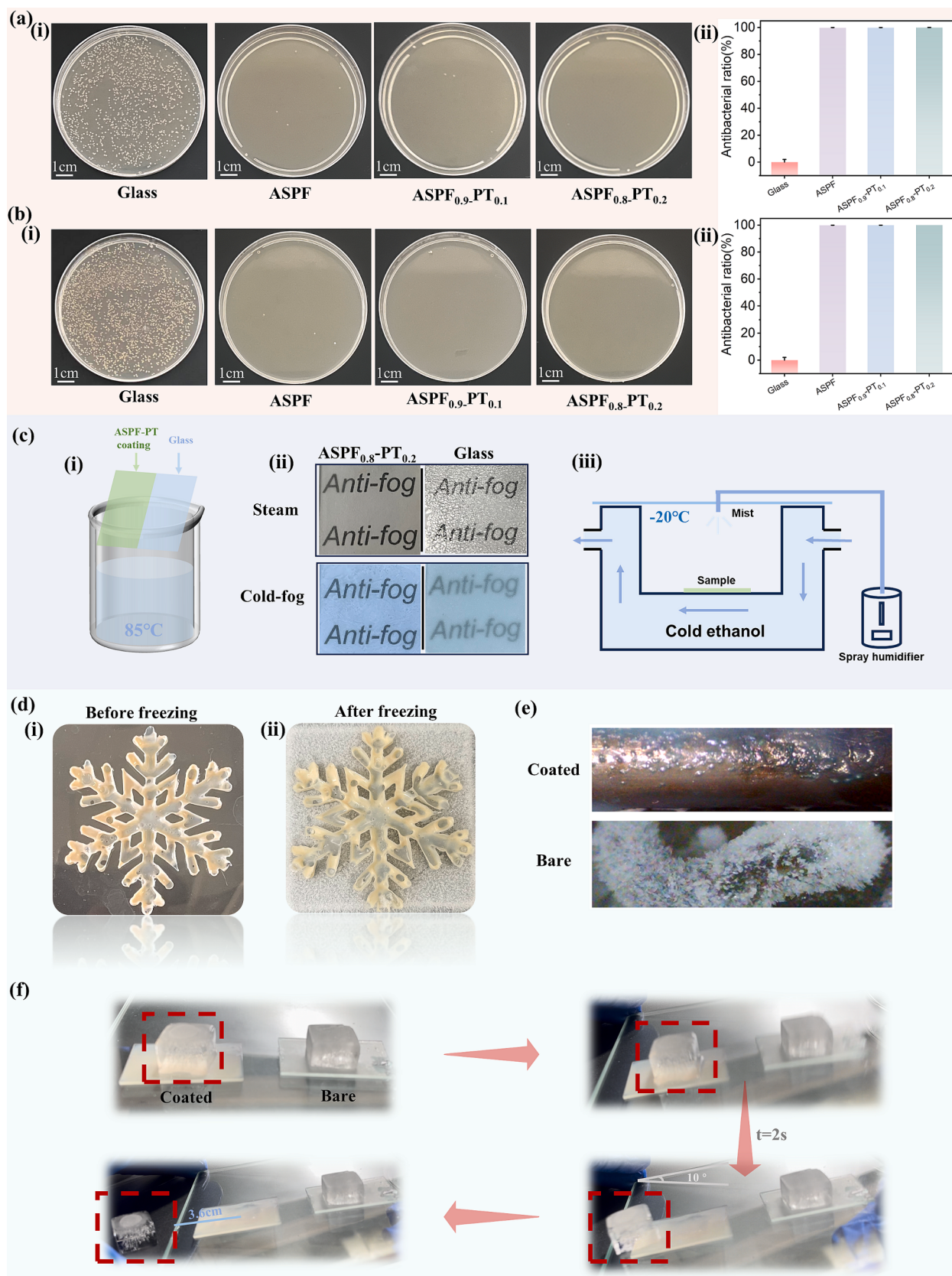


Fig. 9. Antibacterial performance of ASPF, $\text{ASPF}_{0.9}\text{-PT}_{0.1}$, and $\text{ASPF}_{0.8}\text{-PT}_{0.2}$ coatings. (a) *E. coli*. (b) *S. aureus*. (c) (i) Schematic diagram of the steam test, (ii) the anti-fogging property of ASPF-PT coating by steam and cold-fog test. Bare glass was used as a control, (iii) schematic diagram of the cold-fog test. (d) Moldability and anti-frosting capability of ASPF-PT coating ($T = -20^\circ\text{C}$, Humidity $40 \pm 5\%$) (i) before freezing, (ii) after freezing. (e) Anti-frosting performance of bare and $\text{ASPF}_{0.8}\text{-PT}_{0.2}$ coated copper cable ($T = -20^\circ\text{C}$, Humidity $40 \pm 5\%$). (f) Sliding of an ice cube on $\text{ASPF}_{0.8}\text{-PT}_{0.2}$ coating and glass after freezing.

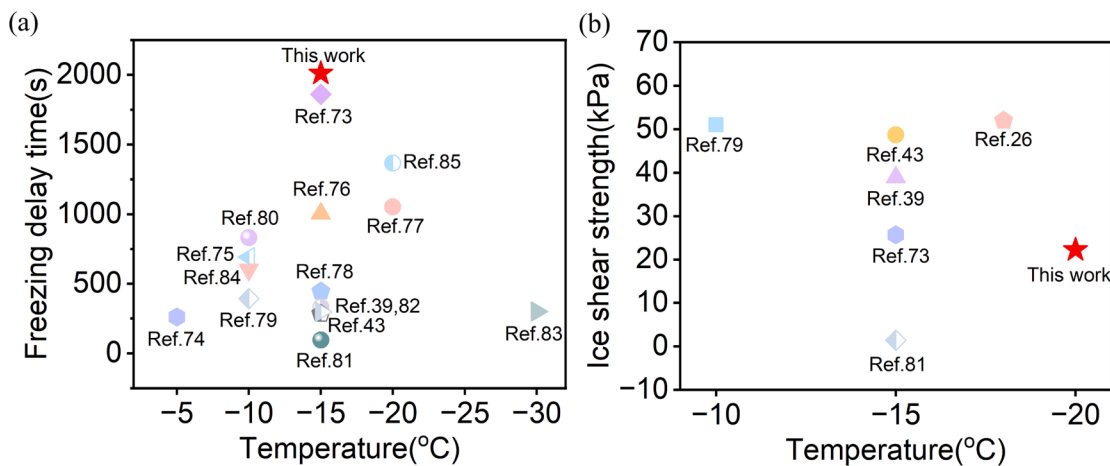


Fig. 10. The comparison of the (a) anti-icing performance and the (b) deicing performance of ASPF-PT coating and other recently-reported works.

$$P_v > P_{v,sat} \exp \left(\frac{\theta}{RT_d} \sqrt{\frac{4\pi}{3} \frac{\sigma^3}{k_B T_d \ln(I)}} (2+m)(1-m)^2 \right) \quad (4)$$

$$m = \cos\theta \quad (5)$$

Frosting occurs mainly due to the diffusion of water molecules on the coating surface and surface temperature conduction. The non-ice binding sites of ASPF-PT coating form a disordered, hydrated layer that inhibits ice nucleation. Additionally, amphoteric sulfobetaine (SBMA) chain segments migrate to the coating surface, enhancing hydrophilicity and modulating interfacial water molecules. This effectively inhibits ice propagation and diffusion by lowering the water freezing point through ionic solvation effects and hydrogen bonding with water molecules [39]. The presence of the hydrated layer also affects heat transfer between the coating surface and the top layer of free water.

3.4. Mechanical performance and the applications

During the actual application of the coating, strong physical external forces such as scratching inevitably occur. The mechanical durability of the coating is evaluated by sandpaper abrasion test (Fig. 8a (i)) and tape peel test (Fig. 8b (i)). As shown in Fig. S10(Supporting Information) and Fig. 8a (ii), b (ii), the ASPF_{0.8}-PT_{0.2} coating maintained its hydrophobicity after 400 sandpaper abrasion tests and 200 tape peel tests with some fluctuation in surface WCA, and SEM shows that the coating still maintains its intact surface morphology (Fig. 8a (iii), b (iii)). The good mechanical durability of the ASPF-PT coating can be attributed to its highly branched fluorinated amphoteric polymer first network (ASPF), which has polar/nonpolar functional groups that can be acted upon by van der Waals forces, hydrogen bonding, and ionic interactions to give the coating good mechanical properties [65,66]. The bionic binder PEI-TA complex as the second network, with its inherent bionic bonding ability [67,68], interacts with the substrate and the ASPF polymer network to build a versatile and stable interpenetrating network coating. Fig. S12 (Supporting Information) shows that the adhesion of the ASPF_{0.8}-PT_{0.2} coating to the substrate is 2.38 MPa. In addition, the thermal decomposition temperature of ASPF and ASPF_{0.8}-PT_{0.2} coating was also evaluated by the thermogravimetric analyzer (TGA). Fig. S11 (Supporting Information) shows the coatings have good thermal stability. Considering the actual use, the coating precursor lotion needs to be stable during storage. Figs. S13 and S14 (Supporting Information) illustrates the particle size distribution and appearance of ASPF copolymers can remain stable within 90 days.

Additionally, the ASPF-PT coating was evaluated for its antibacterial properties in view of the need for functionalization in coating applications. Compared to bare glass, ASPF has some antibacterial performance

with only a small amount of bacterial adhesion on the surface (Fig. 9a, b), which can be attributed to the presence of amphoteric SBMA in the coating [69]. A coating surface coated with ASPF_{0.8}-PT_{0.2} has little bacterial adhesion due to the addition of PEI-TA (Fig. 9a, b-ii), further enhancing the antibacterial properties. By binding to negatively charged elements on the cell membrane surface, the protonated amines in PEI can induce cell membrane rupture and bacterial death [70]. A catechol moiety in TA, on the other hand, can bind to negatively charged surfaces on bacteria, resulting in their death [71]. In addition, we evaluated the anti-fogging property of the coating by steam test and cold-fog test (Fig. 9c (i), (iii)). A highly transparent ASPF-PT coating was prepared by the spin coating method, which meets practical application requirements for an anti-fog coating with high transparency. For the steam test, we placed the bare glass and ASPF-PT coating at 2 °C for 30 min and then held 5 cm above a beaker containing hot water (85 °C) for 10 s. Water vapor covered the surface of the bare glass, making it blurry and reducing transmittance, but the text underneath was still clearly visible with ASPF-PT coating (Fig. 9c(ii)). When the bare glass was placed in the refrigerator at -20 °C and 70 % relative humidity for 30 min, the surface became blurred, which resulted in lower transmission. In contrast, the ASPF-PT coating maintained high transparency. The excellent anti-fog performance can be attributed to the micro-nanostructure of the hydrophobic coating surface (AFM can confirm this), where liquid water is more likely to form smaller droplets on concave and convex surfaces than condensation nuclei such as air. These droplets can become water vapor again under the conversion of the air contained in the coating surface instead of continuing to deposit gradually and thus forming fog.

The ASPF-PT coating also exhibits better formability and frost resistance. According to Fig. 9d, ice crystals fully cover the substrate surface within 12 min at low temperatures and high humidity, but the surface of the snowflake prepared by ASPF-PT was not affected. It can be seen that the copper cable becomes completely frozen within 10 min in Fig. 9e, whereas our anti-icing coating helped prevent frost from forming [72]. Last but not least, we tested the ice-skating performance of the ASPF-PT-coated surface. Fig. 9f shows the coating and glass being placed in the refrigerator to make sure the ice cubes were completely frozen and then removed from the refrigerator. In comparison to the control, in which ice remains on the surface, promisingly, the ice cube easily slid off the coating surface with a visible lubricant water layer after tilting at a slight angle (10°) due to the low ice adhesion.

Fig. 10a, b presents a comparison between the anti-icing and deicing performance of the ASPF-PT coating and other recently reported coatings, which is further summarized in Table S3. Compared with other coatings, the ASPF-PT coating has an extraordinarily long delayed droplet icing time ($DT = 2010$ s) and low ice adhesion ($\tau = 22.2$ kPa).

The above indicates that the ASPF-PT coating achieves a good balance between anti-icing and deicing performance [73–85].

4. Conclusion

In summary, a biomimetic interpenetrating network ASPF-PT anti-icing coating inspired by natural antifreeze proteins (AFPs) in fish was developed. The highly branched fluorinated amphoteric copolymer network ASPF can effectively inhibit ice nucleation ($DT = 2010\text{ s}$, $T_{IN} = -22.1\text{ }^{\circ}\text{C}$), slow down ice propagation, and reduce ice adhesion ($\tau = 22.2\text{ kPa}$) through the synergistic effect of hydrophobicity and ionic specificity, imparting better anti-icing and deicing performance to the coating. In addition, the hydrophilic network PEI-TA bionic binder enabled the coating to exhibit stable mechanical durability and still maintained its hydrophobicity even at extreme conditions such as 400 abrasion cycles and 200 peeling cycles. Unlike some artificial surface microstructures, the interpenetrating network matrix design and inherent advantages of the coating allow it to open up more possibilities in practical applications such as anti-icing, self-cleaning, anti-fogging, and antibacterial. Anti-icing material development could be reshaped by the versatility and functionality of this novel strategy, which simultaneously suppresses ice formation, propagation, and adhesion. Consequently, it may open up new avenues for developing next-generation anti-icing materials as well as real-life applications for icing prevention.

Declaration of competing interest

The authors declare that they have no known competing financial interests or personal relationships that could have appeared to influence the work reported in this paper.

Data availability

Data will be made available on request.

Acknowledgements

This work was supported by the National Natural Science Foundation of China (No. 21978258), Key Research and Development Program of Zhejiang Province (No. 2022C01071) and Hangzhou Science and Technology Development Project (No. 202204T08), Research Funds of Institute of Zhejiang University-Qizhou (IZQ2023RCZX028). The authors would also like to thank the reviewers and editor for their insightful comments, which have improved the quality of the paper.

Appendix A. Supplementary data

Supplementary data to this article can be found online at <https://doi.org/10.1016/j.cej.2023.147836>.

References

- [1] T. Bartels-Rausch, Ten things we need to know about ice and snow, *Nature* 494 (2013) 27–29.
- [2] Z. Azimi Dijvejin, M.C. Jain, R. Kozak, M.H. Zarifi, K. Golovin, Smart low interfacial toughness coatings for on-demand de-icing without melting, *Nat. Commun.* 13 (2022) 5119.
- [3] A. Dhyani, J. Wang, A.K. Halvey, B. Macdonald, G. Mehta, A. Tuteja, Design and applications of surfaces that control the accretion of matter, *Science* 373 (2021) 5010.
- [4] A. Dhyani, W. Choi, K. Golovin, A. Tuteja, Surface design strategies for mitigating ice and snow accretion, *Matter* 5 (2022) 1423–1454.
- [5] Y.Z. Zhuo, J.H. Chen, S.B. Xiao, T. Li, F. Wang, J.Y. He, Z.L. Zhang, Gels as emerging anti-icing materials: a mini review, *Mater. Horiz.* 8 (2021) 3266–3280.
- [6] J. Gao, Y. Zhang, W. Wei, Y. Yin, M. Liu, H. Guo, C. Zheng, P. Deng, Liquid-infused micro-nanostructured MOF coatings (LIMNSMCs) with high anti-icing performance, *ACS Appl. Mater. Interfaces* 11 (2019) 47545–47552.
- [7] Y. Liu, Y. Tian, J. Chen, H. Gu, J. Liu, R. Wang, B. Zhang, H. Zhang, Q. Zhang, Design and preparation of bioinspired slippery liquid-infused porous surfaces with anti-icing performance via delayed phase inversion process, *Colloids Surf., A* 588 (2020) 124384.
- [8] E. Mitridis, T.M. Schutzius, A. Sicher, C.U. Hail, H. Eghlidi, D. Poulikakos, Metasurfaces leveraging solar energy for icephobicity, *ACS Nano* 12 (2018) 7009–7017.
- [9] S.W. Wu, Y.J. Du, Y. Alsaad, D. Wu, M.T. Hua, Y.C. Yan, B.W. Yao, Y.F. Ma, X. Y. Zhu, X.M. He, Superhydrophobic photothermal icephobic surfaces based on candle soot, *Proc. Natl. Acad. Sci. U. S. A.* 117 (2020) 11240–11246.
- [10] R. Chatterjee, H. Bararia, S. Anand, A family of frost-resistant and icephobic coatings, *Adv. Mater.* 34 (2022), 2109930.
- [11] P. Guo, Y. Zheng, M. Wen, C. Song, Y. Lin, L. Jiang, Icephobic/anti-icing properties of micro/nanostructured surfaces, *Adv. Mater.* 24 (2012) 2642–2648.
- [12] Z. Zhang, R. Chen, J. Yu, G. Sun, Q. Liu, J. Liu, J. Zhu, P. Liu, J. Wang, Fluorocarbon-based self-layering interpenetrating polymer-network coatings with anti-fouling and anti-icing properties, *Chem. Eng. J.* 474 (2023), 145540.
- [13] D. Wang, Q. Sun, M.J. Hokkanen, C. Zhang, F.-Y. Lin, Q. Liu, S.-P. Zhu, T. Zhou, Q. Chang, B. He, Q. Zhou, L. Chen, Z. Wang, R.H.A. Ras, X. Deng, Design of robust superhydrophobic surfaces, *Nature* 582 (2020) 55–59.
- [14] L.B. Boinovich, A.M. Emelyanenko, K.A. Emelyanenko, E.B. Modin, Modus operandi of protective and anti-icing mechanisms underlying the design of longstanding outdoor icephobic coatings, *ACS Nano* 13 (2019) 4335–4346.
- [15] W. Zheng, L. Teng, Y. Lai, T. Zhu, S. Li, X. Wu, W. Cai, Z. Chen, J. Huang, Magnetic responsive and flexible composite superhydrophobic photothermal film for passive anti-icing/active deicing, *Chem. Eng. J.* 427 (2022), 130922.
- [16] Z.T. Xie, H. Wang, Y. Geng, M. Li, Q.Y. Deng, Y. Tian, R. Chen, X. Zhu, Q. Liao, Carbon-based photothermal superhydrophobic materials with hierarchical structure enhances the anti-icing and photothermal deicing properties, *ACS Appl. Mater. Interfaces* 13 (2021) 48308–48321.
- [17] A. Azimi Yancheshme, G. Momen, R. Jafari Aminabadi, Mechanisms of ice formation and propagation on superhydrophobic surfaces: a review, *Adv. Colloid Interface Sci.* 279 (2020), 102155.
- [18] Y. Liu, Y. Wu, S. Liu, F. Zhou, Material strategies for ice accretion prevention and easy removal, *ACS Mater. Lett.* 4 (2021) 246–262.
- [19] S. Zhang, F. Zhang, Z. Zhang, G. Li, H. Fu, J. Huang, Y. Wang, Z. Lei, X. Qian, Y. Lai, An electroless nickel plating fabric coated with photothermal Chinese ink for powerful passive anti-icing/icephobic and fast active deicing, *Chem. Eng. J.* 450 (2022), 138328.
- [20] T.-S. Wong, S.H. Kang, S.K.Y. Tang, E.J. Smythe, B.D. Hatton, A. Grinthal, J. Aizenberg, Bioinspired self-repairing slippery surfaces with pressure-stable omniphobicity, *Nature* 477 (2011) 443–447.
- [21] S. Peppou-Chapman, J.K. Hong, A. Waterhouse, C. Neto, Life and death of liquid-infused surfaces: a review on the choice, analysis and fate of the infused liquid layer, *Chem. Soc. Rev.* 49 (2020) 3688–3715.
- [22] H. Zhao, Q. Sun, X. Deng, J. Cui, Earthworm-inspired rough polymer coatings with self-replenishing lubrication for adaptive friction-reduction and antifouling surfaces, *Adv. Mater.* 30 (2018), 1802141.
- [23] Q. Rao, J. Zhang, X. Zhan, F. Chen, Q. Zhang, UV-driven self-replenishing slippery surfaces with programmable droplet-guiding pathways, *J. Mater. Chem. A* 8 (2020) 2481–2489.
- [24] Y. Liu, W. Sun, K. Feng, Y. Wu, B. Yu, S. Liu, F. Zhou, Sebaceous gland-inspired self-lubricated de-icing coating by continuously secreting lubricants, *Prog. Org. Coat.* 174 (2023), 107311.
- [25] Y. Jin, C. Wu, Y. Yang, J. Wu, Z. He, J. Wang, Inhibiting condensation freezing on patterned polyelectrolyte coatings, *ACS Nano* 14 (2020) 5000–5007.
- [26] R. Wang, C. Cheng, H. Wang, Q. Tao, D. Wang, A simple poly(Vinyl sulfonate) coating for all-purpose, self-cleaning applications: molecular packing density-defined surface superhydrophilicity, *Adv. Funct. Mater.* 33 (2023), 2301085.
- [27] P. Irajizad, A. Al-Bayati, B. Eslami, T. Shafquat, M. Nazari, P. Jafari, V. Kashyap, A. Masoudi, D. Araya, H. Ghasemi, Stress-localized durable icephobic surfaces, *Mater. Horiz.* 6 (2019) 758–766.
- [28] F. Wang, Y. Zhuo, Z. He, S. Xiao, J. He, Z. Zhang, Dynamic anti-icing surfaces (DAIS), *Adv. Sci.* 8 (2021), 2101163.
- [29] S. Schöder, H. Reichert, H. Schröder, M. Mezger, J.S. Okasinski, V. Honkimäki, J. Bilgram, H. Dosch, Radiation-induced premelting of ice at silica interfaces, *Phys. Rev. Lett.* 103 (2009), 095502.
- [30] A.L. Devries, D.E. Wohlschlag, Freezing resistance in some antarctic fishes, *Science* 163 (1969) 1073.
- [31] A.P. Esser-Kahn, V. Trang, M.B. Francis, Incorporation of antifreeze proteins into polymer coatings using site-selective bioconjugation, *J. Am. Chem. Soc.* 132 (2010) 13264–13269.
- [32] H.G. Yang, C. Ma, K.Y. Li, K. Liu, M. Loznik, R. Teeuwen, J.C.M. van Hest, X. Zhou, A. Herrmann, J.J. Wang, Tuning ice nucleation with supercharged polypeptides, *Adv. Mater.* 28 (2016) 5008–5012.
- [33] Y.L. Sun, G. Giubertoni, H.J. Bakker, J. Liu, M. Wagner, D.Y.W. Ng, A.L. Devries, K. Meister, Disaccharide residues are required for native antifreeze glycoprotein activity, *Biomacromolecules* 22 (2021) 2595–2603.
- [34] Z. He, C. Wu, M. Hua, S. Wu, D. Wu, X. Zhu, J. Wang, X. He, Bioinspired multifunctional anti-icing hydrogel, *Matter* 2 (2020) 723–734.
- [35] R.M. Dou, J. Chen, Y.F. Zhang, X.P. Wang, D.P. Cui, Y.L. Song, L. Jiang, J.J. Wang, Anti-icing coating with an aqueous lubricating layer, *ACS Appl. Mater. Interfaces* 6 (2014) 6998–7003.
- [36] K. Liu, C. Wang, J. Ma, G. Shi, X. Yao, H. Fang, Y. Song, J. Wang, Janus effect of antifreeze proteins on ice nucleation, *Proc. Natl. Acad. Sci.* 113 (2016) 14739–14744.

- [37] Z. Ma, Y. Liu, K. Feng, J. Wei, J. Liu, Y. Wu, X. Pei, B. Yu, M. Cai, F. Zhou, "Brush-like" amphiphilic polymer for environmental adaptive coating, *ACS Appl. Mater. Interfaces* 14 (2022) 18901–18909.
- [38] W. Huang, J. Huang, Z. Guo, W. Liu, Icophobic/anti-icing properties of superhydrophobic surfaces, *Adv. Colloid Interface Sci.* 304 (2022), 102658.
- [39] S. Tian, R. Li, X. Liu, J. Wang, J. Yu, S. Xu, Y. Tian, J. Yang, L. Zhang, Inhibition of defect-induced ice nucleation, propagation, and adhesion by bioinspired self-healing anti-icing coatings, *Research* 6 (2023) 0140.
- [40] X. Peng, Y. Li, T.J. Li, Y.C. Li, Y.R. Deng, X. Xie, Y. Wang, G. Li, L.M. Bian, Coacervate-derived hydrogel with effective water repulsion and robust underwater bioadhesion promotes wound healing, *Adv. Sci.* 9 (2022), 2203890.
- [41] Z. Wang, L. Guo, H. Xiao, H. Cong, S. Wang, A reversible underwater glue based on photo- and thermo-responsive dynamic covalent bonds, *Mater. Horiz.* 7 (2020) 282–288.
- [42] H.F. Wang, X.P. Li, Y. Jiang, M.H. Li, Q. Xiao, T. Zhao, S. Yang, C.H. Qi, P.P. Qiu, J. P. Yang, Z. Jiang, W. Luo, A universal single-atom coating strategy based on tannic acid chemistry for multifunctional heterogeneous catalysis, *Angew Chem Int Edit* 61 (2022), 202200465.
- [43] R. Li, S. Tian, Y. Tian, J. Wang, S. Xu, K. Yang, J. Yang, L. Zhang, An Extreme-environment-resistant self-healing anti-icing coating, *Small* 19 (2022), 2206075.
- [44] Y. Zhang, A. Takahara, Synthesis and surface properties of amphiphilic copolymer consisting of hydrophobic perfluorocarbon and hydrophilic zwitterionic blocks, *Polymer* 230 (2021), 124029.
- [45] L.M. Yi, K. Xu, G.Y. Xia, J.W. Li, W.X. Li, Y. Cai, New protein-resistant surfaces of amphiphilic graft copolymers containing hydrophilic poly(ethylene glycol) and low surface energy fluorosiloxane side-chains, *Appl. Surf. Sci.* 480 (2019) 923–933.
- [46] L.M. Yi, X.M. Meng, X.P. Tian, W. Zhou, R.W. Chen, Wettability of electrospun films of microphase-separated block copolymers with 3,3-trifluoropropyl substituted siloxane segments, *J Phys Chem C* 118 (2014) 26671–26682.
- [47] P. Irajizad, M. Hasnain, N. Farokhnia, S.M. Sajadi, H. Ghasemi, Magnetic slippery extreme icophobic surfaces, *Nat. Commun.* 7 (2016) 13395.
- [48] Q. Yang, Z.W. Zhu, S. Tan, Y.M. Luo, Z.Z. Luo, How micro-/nanostructure evolution influences dynamic wetting and natural deicing abilities of bionic lotus surfaces, *Langmuir* 36 (2020) 4005–4014.
- [49] W. Niu, G.Y. Chen, H. Xu, X. Liu, J. Sun, Highly transparent and self-healable solar thermal anti-/deicing surfaces: when ultrathin mxene multilayers marry a solid slippery self-cleaning coating, *Adv. Mater.* 34 (2022), 2108232.
- [50] W.W. Zheng, J.Y. Huang, X.R. Zang, X.F. Xu, W.L. Cai, Z.Q. Lin, Y.K. Lai, Judicious design and rapid manufacturing of a flexible, mechanically resistant liquid-like coating with strong bonding and antifouling abilities, *Adv. Mater.* 34 (2022), 2204581.
- [51] Y. Wu, X. Tan, Y. Wang, F. Tao, M. Yu, X. Chen, Nonfluorinated, transparent, and antireflective hydrophobic coating with self-cleaning function, *Colloids Surf., A* 634 (2022), 127919.
- [52] L. Jiang, P. Hou, S. He, M. Han, P. Xiang, T. Xiao, X. Tan, The robust superhydrophobic SiO₂/Diatomite/PDMS/KH-570/Me-MQ composite coating for self-cleaning application of building surface, *Colloids Surf., A* 634 (2022), 127936.
- [53] A. Tuteja, W. Choi, M. Ma, J.M. Mabry, S.A. Mazzella, G.C. Rutledge, G. H. McKinley, R.E. Cohen, Designing superoleophobic surfaces, *Science* 318 (2007) 1618–1622.
- [54] S. Pan, R. Guo, M. Björnalm, J.J. Richardson, L. Li, C. Peng, N. Bertleff-Zieschang, W. Xu, J. Jiang, F. Caruso, Coatings super-repellent to ultralow surface tension liquids, *Nat. Mater.* 17 (2018) 1040–1047.
- [55] T. Wu, W. Xu, X. Li, Y. Du, M. Sheng, H. Zhong, H. Xie, J. Qu, Bioinspired micro/nanostructured polyethylene/poly(ethylene oxide)/graphene films with robust superhydrophobicity and excellent antireflectivity for solar-thermal power generation, thermal management, and afterheat utilization, *ACS Nano* 16 (2022) 16624–16635.
- [56] S. Jiang, Y. Diao, H. Yang, Recent advances of bio-inspired anti-icing surfaces, *Adv. Colloid Interface Sci.* 308 (2022), 2108232.
- [57] X. Xu, V.V. Jerca, R. Hoogenboom, Bio-inspired hydrogels as multi-task anti-icing hydrogel coatings, *Chem* 6 (2020) 820–822.
- [58] J. Yang, R. Wang, X. Zhang, F. Long, T. Zhou, L. Liu, Self-roughened superhydrophobic polydopamine coating with excellent self-cleaning, anti-corrosion, and UV shielding performances, *J. Appl. Polym. Sci.* 139 (2022) 52114.
- [59] Z. Zhang, X.-Y. Liu, Control of ice nucleation: freezing and antifreeze strategies, *Chem. Soc. Rev.* 47 (2018) 7116–7139.
- [60] Y. Shen, X. Wu, J. Tao, C. Zhu, Y. Lai, Z. Chen, Icophobic materials: Fundamentals, performance evaluation, and applications, *Prog. Mater Sci.* 103 (2019) 509–557.
- [61] Y. Wu, L. Dong, X. Shu, Y. Yang, P. Feng, Q. Ran, Recent advancements in photothermal anti-icing/deicing materials, *Chem. Eng. J.* 469 (2023), 143924.
- [62] B. Liang, G. Zhang, Z. Zhong, Y. Huang, Z. Su, Superhydrophobic anti-icing coatings based on polyzwitterion brushes, *Langmuir* 35 (2018) 1294–1301.
- [63] J.B. Boreyko, C.P. Collier, Delayed frost growth on jumping-drop superhydrophobic surfaces, *ACS Nano* 7 (2013) 1618–1627.
- [64] S. Nath, J.B. Boreyko, On localized vapor pressure gradients governing condensation and frost phenomena, *Langmuir* 32 (2016) 8350–8365.
- [65] C. Wang, P. Chen, Y. Wang, T. Chen, M. Liu, M. Zhang, Y. Fu, J. Xu, J. Fu, Synergistic cation-anion regulation of polysulfides by zwitterionic polymer binder for lithium-sulfur batteries, *Adv. Funct. Mater.* 32 (2022), 2204451.
- [66] R.H. Gao, Q. Zhang, Y. Zhao, Z.Y. Han, C.B. Sun, J.Z. Sheng, X.W. Zhong, B. A. Chen, C. Li, S.Y. Ni, Z.H. Piao, B.H. Li, G.M. Zhou, Regulating polysulfide redox kinetics on a self-healing electrode for high-performance flexible lithium-sulfur batteries, *Adv. Funct. Mater.* 32 (2022), 2110313.
- [67] W. Zhang, R. Wang, Z. Sun, X. Zhu, Q. Zhao, T. Zhang, A. Cholewinski, F. Yang, B. Zhao, R. Pinnaratip, P.K. Foroshani, B.P. Lee, Catechol-functionalized hydrogels: biomimetic design, adhesion mechanism, and biomedical applications, *Chem. Soc. Rev.* 49 (2020) 433–464.
- [68] X. Peng, X. Xu, Y.R. Deng, X. Xie, L.M. Xu, X.Y. Xu, W.H. Yuan, B.G. Yang, X. F. Yang, X.F. Xia, L. Duan, L.M. Bian, Ultrafast self-gelling and wet adhesive powder for acute hemostasis and wound healing, *Adv. Funct. Mater.* 31 (2021), 2102583.
- [69] D.H. Wang, J.K. Xu, J.Y. Tan, J.L. Yang, S.X. Zhou, In situ generation of amphiphilic coatings based on a self-catalytic zwitterionic precursor and their antifouling performance, *Chem. Eng. J.* 422 (2021), 130115.
- [70] C. Yang, J. Dawulieti, K.B. Zhang, C.X. Cheng, Y.W. Zhao, H.Z. Hu, M. Li, M. Zhang, L. Chen, K.W. Leong, D. Shao, An injectable antibiotic hydrogel that scavenges proinflammatory factors for the treatment of severe abdominal trauma, *Adv. Funct. Mater.* 32 (2022), 2111698.
- [71] R.Y. Li, Y.Y. Fan, L.L. Liu, H.N. Ma, D.Y. Gong, Z.H. Miao, H. Wang, Z.B. Zha, Ultrathin hafnium disulfide atomic crystals with ROS-scavenging and colon-targeting capabilities for inflammatory bowel disease treatment, *Acs Nano* 16 (2022) 15026–15041.
- [72] Y.K. Jian, S. Handschuh-Wang, J.W. Zhang, W. Lu, X.C. Zhou, T. Chen, Biomimetic anti-freezing polymeric hydrogels: keeping soft-wet materials active in cold environments (Sep, 10.1039/d0mh01029d, 2020), *Mater. Horiz.* 7 (2020) 3339–3339.
- [73] Y. Wu, X. Shu, Y. Yang, W. She, L. Dong, Q. Ran, Fabrication of robust and room-temperature curable superhydrophobic composite coatings with breathable and anti-icing performance, *Chem. Eng. J.* 463 (2023), 142444.
- [74] J. Wei, B. Li, N. Tian, J. Zhang, W. Liang, J. Zhang, Scalable robust superamphiphobic coatings enabled by self-similar structure, protective micro-skeleton, and adhesive for practical anti-icing of high-voltage transmission tower, *Adv. Funct. Mater.* 32 (2022), 2206014.
- [75] Z. Lin, C. Ma, Z. Ma, L. Gao, W. Chen, G. Chen, Laser etching ultra-black coating with novel anti-icing performance, *Chem. Eng. J.* 466 (2023), 143067.
- [76] H. He, W. Huang, Z. Guo, Superhydrophobic and photothermal SiC/TiN durable composite coatings for passive anti-icing/active de-icing and de-frosting, *Mater. Today Phys.* 30 (2023), 100927.
- [77] J. Wang, P. Li, P. Yu, T. Leydecker, I.S. Bayer, D. Losic, A. Neogi, Z. Wang, Efficient photothermal deicing employing superhydrophobic plasmonic MXene composites, *Adv. Compos. Hybrid Mater.* 5 (2022) 3035–3044.
- [78] Z. Xie, H. Wang, M. Li, Y. Tian, Q. Deng, R. Chen, X. Zhu, Q. Liao, Photothermal trap with multi-scale micro-nano hierarchical structure enhances light absorption and promote photothermal anti-icing/deicing, *Chem. Eng. J.* 435 (2022), 135025.
- [79] J. Li, W. Jiao, Y. Wang, Y. Yin, X. He, Spraying pressure-tuning for the fabrication of the tunable adhesion superhydrophobic coatings between Lotus effect and Petal effect and their anti-icing performance, *Chem. Eng. J.* 434 (2022), 134710.
- [80] B. Wang, P. Yu, Q. Yang, Z. Jing, W. Wang, P. Li, X. Tong, F. Lin, D. Wang, G.E. Lio, R. Caputo, O. Avalos-Ovando, A.O. Govorov, H. Xu, Z.M. Wang, Upcycling of biomass waste into photothermal superhydrophobic coating for efficient anti-icing and deicing, *Mater. Today Phys.* 24 (2022), 100683.
- [81] L. Wang, G. Jiang, Z. Tian, C. Chen, X. Hu, R. Peng, H. Zhang, P. Fan, M. Zhong, Superhydrophobic microstructures for better anti-icing performances: open-cell or closed-cell? *Mater. Horiz.* 10 (2023) 209–220.
- [82] L. Wang, Z. Tian, G. Jiang, X. Luo, C. Chen, X. Hu, H. Zhang, M. Zhong, Spontaneous dewetting transitions of droplets during icing & melting cycle, *Nat. Commun.* 13 (2022) 378.
- [83] W.-L. Zhou, T. Wu, Y. Du, X.-H. Zhang, X.-C. Chen, J.-B. Li, H. Xie, J.-P. Qu, Efficient fabrication of desert beetle-inspired micro/nano-structures on polypropylene/graphene surface with hybrid wettability, chemical tolerance, and passive anti-icing for quantitative fog harvesting, *Chem. Eng. J.* 453 (2023), 139784.
- [84] H. Xie, W.H. Xu, Y. Du, J. Gong, R. Niu, T. Wu, J.P. Qu, Cost-effective fabrication of micro-nanostructured superhydrophobic polyethylene/graphene foam with self-floating, optical trapping, acid-/alkali resistance for efficient photothermal deicing and interfacial evaporation, *Small* 18 (2022), 2200175.
- [85] M.L. Yu, X. Li, X.Y. Tan, X.B. Chen, Fluorine-free preparation of a superhydrophobic coating with anti-icing properties, mechanical durability and self-cleaning effect, *Soft Matter* 19 (2023) 766–775.